ARTICLE

Mutant GTF2I induces cell transformation and metabolic alterations in thymic epithelial cells

In-Kyu Kim [1] · Guanhua Rao[1] · Xiaoliang Zhao[1] · Ruzong Fan[1] · Maria Laura Avantaggiati[1] · Yisong Wang[1,2] · Yu-Wen Zhang[1] · Giuseppe Giaccone[1]

Abstract

The pathogenesis of thymic epithelial tumors (TETs) is poorly understood. Recently we reported the frequent occurrence of a missense mutation in the *GTF2I* gene in TETs and hypothesized that *GTF2I* mutation might contribute to thymic tumorigenesis. Expression of mutant TFII-I altered the transcriptome of normal thymic epithelial cells and upregulated several oncogenic genes. *Gtf2i* L424H knockin cells exhibited cell transformation, aneuploidy, and increase tumor growth and survival under glucose deprivation or DNA damage. *Gtf2i* mutation also increased the expression of several glycolytic enzymes, cyclooxygenase-2, and caused modifications of lipid metabolism. Elevated cyclooxygenase-2 expression by *Gtf2i* mutation was required for survival under metabolic stress and cellular transformation of thymic epithelial cells. Our findings identify *GTF2I* mutation as a new oncogenic driver that is responsible for transformation of thymic epithelial cells.

Introduction

Thymic epithelial tumors (TETs) are uncommon, primary neoplasms of the anterior mediastinum derived from the thymic epithelium, with an annual incidence ranging from 1.3 to 3.2/million [1, 2]. The World Health Organization histologic classification distinguishes thymomas (A, AB, B1, B2, and B3), from thymic carcinomas (TC) [3]. However, the complex and frequently mixed histomorphology renders TETs one of the most challenging tumors to classify histologically [4]. Prognosis worsens progressively from type A to

TC: 10-year survival is 90–95% in types A through B1, and 5-year survival rates for B2, B3, and TC are 75%, 70%, and 48%, respectively [5]. The etiology of TETs is obscure, aside from the controversial reports of an association with EB virus infection [6], and thymomas can be commonly associated with autoimmune diseases such as myasthenia gravis. In addition, the genetic/molecular aberrations associated with TETs are largely unknown and a lack of appropriate pre-clinical models hinders investigation of the cause of TETs.

Using exome and RNA sequencing, we recently reported a highly recurrent unique somatic mutation of *GTF2I* in the least aggressive thymomas, and predicted that *GTF2I* mutation is necessary for the founder tumor clone in thymus [7]. These findings were later confirmed by the The Cancer Genome Atlas (TCGA) program [8]. *GTF2I* encodes TFII-I, a transcription factor, and there are currently at least five known splice variants of *GTF2I* recognized in the human genome. We discovered that the β and δ isoforms of TFII-I are predominantly expressed in TETs; these isoforms are known as negative or positive regulators in gene transcription with distinct subcellular localization in response to mitogen signal [9]. The observed *GTF2I* T1211A (L424H) missense mutation at chr.7:74146970 leads to p.Leu404His and p.Leu383His substitution in the β and δ isoforms of TFII-I, respectively.

The human TFII-I protein belongs to a family of transcription factors, consisting of three related genes (*GTF2I*

✉ In-Kyu Kim
  ingyu.kim80@gmail.com

✉ Giuseppe Giaccone
  gg496@georgetown.edu

1   Department of Oncology, Lombardi Comprehensive Cancer Center, Georgetown University, Washington, DC 20057, USA

2   Basic and Mechanistic Research Branch, Division of Extramural Research, National Center for Complementary and Integrative Health (NCCAIH), NIH, Bethesda, MD 20892, USA

and its pseudogenes *GTF2IP1*, and LOC100093631) that are located in close proximity on the long arm of chromosome 7. A portion of the long arm of chromosome 7 is deleted in a haplo-insufficient manner in Williams–Beuren syndrome, a genetic disorder characterized by marked defects in neurological and cardiovascular development [10]. Originally TFII-I was identified as a novel type of transcription initiation factor that binds to multiple promoter elements including a pyrimidine-rich initiator (Inr). TFII-I is a multifunctional protein associated with the transcriptional regulation of several genes that control cell proliferation, cell cycle, angiogenesis, cellular stress response, and development, through sequence-specific DNA binding [11]. Despite the many functions of TFII-I, alterations of *GTF2I* in tumors have not been reported until recently.

Here, we investigated the effects of *GTF2I* mutation on transcriptional regulation, and several biological and metabolic processes involved in tumorigenesis. We demonstrated that the mutant TFII-I (mtTFII-I) expression in thymic epithelial cells (TECs) results in upregulation of oncogenes and cell transformation. *Gtf2i* mutation conferred cell transformation and survival advantage through COX-2 expression in response to metabolic stress and promoted tumor growth in vivo.

Materials and methods

Cell culture

All mouse normal TEC lines (TEC71, TEC100.4, TEC41.2, TEC301, and Z210r; a kind gift from Dr. Julien Sage, Stanford University) were maintained in RPMI-1640 (Thermo Fisher; Waltham, MA, USA), and 293T cells were grown in DMEM supplemented with 10% FBS (Thermo Fisher). NIH-3T3 cells were maintained in DMEM supplemented with 10% bovine calf serum (Thermo Fisher). All cell lines were cultivated as monolayer in each optimal medium with 2% penicillin–streptomycin (Thermo Fisher). Doxycycline Hydrochloride was purchased from Thermo Fisher and solubilized in distilled water. For metabolic studies, RPMI-1640 with no glucose, dialyzed FBS, and D-glucose from Thermo Fisher were used. Cisplatin and Doxorubicin were purchased from Selleckchem (Houston, TX, USA).

Production of lentiviral particles

293T cells were plated in 10 cm culture dishes and were transfected with 6 μg lentiviral vector, 0.6 μg lenti-Rev/-PM2/-Tat, and 1.2 μg lenti-Vsv-G at the ratio 10:1:1:1:2 using X-tremeGENE 9 (SIGMA; St. Louis, MO, USA), the

next day. Growth medium was changed after 24 h and virus-containing medium was collected between 36 and 48 h after transfection and filtered through 0.45 μm low-binding PES membrane. Virus particles were stored at −80 °C until use.

Doxycycline inducible system

Mutated *GTF2I* [7] was amplified by PCR using the following primers: 5′-CACCATGGCCCAAGTTGCAATGT C-3′, and 5′-AAACCACGTGGGGTCTGGTTCTTG-3′. PCR fragments were clone into the pENTR/D-TOPO (Thermo Fisher), and subsequently moved into a pLIX402 lentiviral vector (Addgene; Cambridge, MA, USA) using Gateway LR Clonase II Enzyme mix (Thermo Fisher) according to the manufacturer's instructions. The insert sequence in the plasmid was sequenced, and confirmed HA-tag expression under the control of doxycycline in 293T cells first. Mouse thymic epithelial cells (mTECs) were seeded ($3–4 \times 10^4$) in six-well plates and infected with lentivirus the next day. After 48 h infection, 3–5 μg/mL puromycin was used for selection and puromycin-resistant single clones were picked by pyrex cloning cylinder (SIGMA). Five micrograms of the pLIX402 plasmids with mutated *GTF2I* isoforms were transfected into TEC100.4 cells using the Nucleofector Kit V (Lonza; Salisbury, MD, USA) with Nucleofector 2b device under T-30 program. After 48 h transfection, 3 μg/mL puromycin was used for selection and puromycin-resistant single clones were picked by Pyrex cloning cylinder.

Establishment of stable knockdown (KD) cells

pLKO.1 from Addgene (#8453), two COX-2 shRNA (TRCN0000067941 and TRCN0000067939), PFKFB2 shRNA (TRCN0000361450 and TRCN0000361451), PFKP (TRCN0000025962 and TRCN0000025916), and ENO2 shRNA (TRCN0000340138 and TRCN0000340139) were purchased from Sigma. Cells were infected with shRNA lentiviral particles and selected by 10 μg/ml of puromycin. Cells transfected with pLKO.1 were used as a control.

Western blot analysis and antibodies

Cells were harvested and lysed in $1 \times$ lysis buffer [60 mM Tris (pH 7.4), 25 mM HEPES, 150 mM NaCl, 10% glycerol, 5 mM EDTA, 1% Triton X-100, 5 mM Na3VO4, 50 mM NaF, two pills protease inhibitor cocktail tablets] on ice for 45 min and centrifuged at 15,000 rpm for 15 min. Cell lysates were separated by 4–20% SDS-PAGE and transferred to a PVDF membrane. Subsequently, the membrane was incubated in TBST supplemented with 5% nonfat dry milk or BSA and probed with the appropriate primary antibodies. The bound antibodies were visualized with a

suitable secondary antibody conjugated with horseradish peroxidase using enhanced chemiluminescence reagent WESTSAVE up by PXi6 imaging system. The following primary antibodies were used: Aldolase A (8060, Cell Signaling), Bcl2 (sc-7382, Santa Cruz), Bcl-xL (sc-8392, Santa Cruz), cleaved Caspase-3 (9661, Cell Signaling), COX-1 (4841, Cell Signaling), COX-2 (12282, Cell Signaling), Enolase-1 (3810, Cell Signaling), Enolase-2 (8171, Cell Signaling), p-Erk1/2 (9101, Cell Signaling), Erk1/2 (9102, Cell Signaling), FGFBP (sc-68177, Santa Cruz), c-fos (sc-52, Santa Cruz), GAPDH (5174, Cell Signaling), HA (H9658, SIGMA), Hexokinase I (2024, Cell Signaling), Hexokinase II (2867, Cell Signaling), γH2AX (613402, BioLegend), c-kit (sc-168 and sc-365504, Santa Cruz), Lactate Dehydrogenase (ab52488, Abcam), Mdm2 (sc-965, Santa Cruz), c-myc (ab51154, Abcam), PARP (9542, Cell Signaling), cleaved PARP (9544, Cell Signaling), PDCD4 (9535, Cell Signaling), PDHK1 (3820, Cell Signaling), PFKP (8164, Cell Signaling), PFKFB2 (13045, Cell Signaling), PFKFB3 (13123, Cell Signaling), PGAM1 (12098, Cell Signaling), PKM2 (4053, Cell Signaling), PKM1/2 (3190, Cell Signaling), p16 (ab189034, Abcam), p21 (556431, BD Bioscience), p53 (2524, Cell Signaling), phospho-p53 (9284, Cell Signaling), Slug (9585, Cell Signaling), Snail (sc-271977, Santa Cruz), TFII-I (4562, Cell Signaling), TWIST (GTX127310, GeneTex), α-Tubulin (T6199, SIGMA), VEGFC (ab9546, Abcam), VEGFD (sc-373866, Santa Cruz), VEGFR1 (ab32152, Abcam), VEGFR2 (sc-504, Santa Cruz), and WNT2B (sc-98737, Santa Cruz).

Immunostaining

Cells were seeded on glass coverslips in 12-well plates. In the doxycycline inducible system, cells were incubated with/without 2 μg/ml doxycycline for 24 h. After cells were fixed with 4% paraformaldehyde and permeabilized with 0.1% Triton X-100, cells were incubated with 1% BSA (in PBS). Then, cells were incubated with primary antibody: HA (1:200 #H9658, SIGMA), Vimentin (1:200 #5741, Cell Signaling), V5 (R960–25, Thermo Fisher), or Texas Red-X phalloidin (1:50 #T7471, Thermo Fisher) in 1% BSA for overnight at 4 °C. Following PBS washing, cells were incubated with Alexa Fluor 488 (#A-11029, Thermo Fisher) or Alexa Fluor 555 conjugate (#A-21422, Thermo Fisher) secondary antibody for 1 h at room temperature. Labeled cells were rinsed with PBS and mounted in VECTA-SHIELD Hardset Mounting Medium (#H-1500, Vector Laboratories; Burlingame, CA, USA) or ProLong Gold Antifade Reagent with DAPI (#8961, Cell Signaling). The cells were examined by immunofluorescent microscope (Olympus).

Quantitative RT-PCR (qRT-PCR)

Total RNA was isolated using the RNeasy Plus Mini Kit (#74134, QIAGEN; Germantown, MD, USA) according to the manufacturer's instructions. qRT-PCR was carried out using ABI 7900HT Fast Real-time PCR system (Applied Biosystems) and the QuantiTect SYBR Green RT-PCR Kit (#204243, QIAGEN). Reactions were run in three independent experiments ($n = 3$). The used primers are described in Supplementary Table S1.

Gene expression microarray analysis

Total RNA was prepared using the RNeasy Plus Mini Kit (QIAGEN) according to manufacturer's protocol. The TEC100.4 + pLIX402/TFII-I-βmt and -δmt inducible cells were treated with/without doxycycline, and total RNA was prepared 24 h later. Microarrays were performed at the Genomics and Epigenomics Shared Resources at Georgetown University: total RNAs were subjected to hybridization on the Agilent SurePrint G3 mouse gene expression V2 $8 × 60$ K microarray kit (Agilent; Savage, MD, USA) according to the manufacturer's protocol. Briefly, 200 ng of total RNA was used to generate fluorescent cRNA using the Agilent Low Input Quick Amp labeling Kit, One-Color. The cRNA was hybridized to the array and scanned using the Agilent G2505C DNA Scanner System, and the data were extracted using Agilent Feature Extraction Software v11.5.11. The web-based functional annotation tool DAVID was used for functional gene enrichment analysis of differentially expressed genes (>1.5-fold).

Cell proliferation assay

Cells were placed in 6 or 10 cm culture dishes and viable cells were counted with a hemocytometer or TC20 automated cell counter (Bio-rad; Hercules, CA, USA) using trypan blue staining at indicated time points. The Cell Counting Kit-8 (VitaScientific; College Park, MD, USA) was also used to further determine cell proliferation following the manufacturer's manual. One thousand cells were plated in 96-well plates and incubated for indicated time point. CCK-8 solution was added and followed by incubation for 1 h at 37 °C. The absorbance at 450 nm was measured by Glomax.

Cell cycle analysis

Cells were plated in 10 cm dishes and incubated overnight. Next day, growth medium was changed with fresh medium containing normal or 5 mM glucose and incubated for 72 h. Following incubation, cells were fixed with ethanol and washed with cold PBS. After centrifugation, cell pellets

were mixed with Propidium iodide (PI) solution and incubated for 30 min at room temperature in dark environment. Cell cycle was analyzed using FACSCalibur Flow Cytometer (BD Bioscience). Acquired data were processed using the FlowJo software (Tree Star). For aneuploidy analysis, DNA content was defined as DNA Index (DI) and mouse spleen cells were used as internal control. DNA aneuploidy was characterized by the DI (diploid: $DI = 1$, aneuploid: $DI \neq 1$) and obtained by dividing additional G1 peak by the residual G1 peak in the sample.

Annexin V/PI staining

Cells were washed with PBS and harvested by trypsinization, resuspended in binding buffer, and then incubated with Annexin V-FITC antibody for 20 min in dark environment. PI was added before proceeding to flow cytometry analysis.

TUNEL assay

In Situ Cell Death Detection Kit (SIGMA) was used to assess cell apoptosis following the manufacturer's instructions. Cells were plated in six-well plates with cover slip and incubated overnight. Next day, growth medium was replaced with normal or 5 mM glucose medium and cells were incubated for 48–72 h. After fixation (4% paraformaldehyde) and permeabilization, cells were stained using the TUNEL reaction mixture in dark environment. Labeled cells were mounted in VECTASHIELD Hardset Mounting Medium and examined by immunofluorescence microscope. TUNEL-positive cells were counted to quantify the apoptosis rate.

CRISPR/Cas9n-mediated engineering of the normal mTECs genome

Cells (1×10^6) were co-transfected with 1.5 μg of each two gRNAs (pU6-gRNA, SIGMA), 4 μg of pSpCas9n (D10A nickase mutant, PX462, Addgene), and 25 μg of donor DNA (3080 bp). Transfection was performed using the Amaxa nucleofector kit V with T-30 program at six-well culture plate. The oligonucleotides used for gRNA were: 5′-ACGTCGACGGCCTTCTAAA, 5′-GAGAGGATATTG CTGGCGA-3′. Because of the low efficiency with knockin (KI) based on homology-directed repair strategy with CRISPR system, we could not get correct clone while we screened hundreds clones with single-stranded oligodeoxynucleotides used as the homologous recombination (HR) donor template. Then we adopted a new strategy to use Scr7, a DNA ligase IV inhibitor [12], with double-strand DNA which has a new restriction enzyme site (SphI) as a HR template. After 6 h incubation, the culture medium was changed with fresh medium containing 1 μM SCR7, and then incubated for 72 h. Puromycin (8 μg/ml) was used for

selection and single colonies were picked and transferred to 96- or 48-well plates to expand. Genomic DNAs of all clones were isolated by using the GenElute™ mammalian genomic DNA miniprep kit (SIGMA) and target region was amplified by PCR. CRISPR/Cas9n-mediated HR was confirmed by two-step PCR and restriction enzyme digestion with SphI. Two primers set (5′-CATGCTTGTTCTCAGTGC TTTC-3′, 5′-CCCTCGTAAGGGCTATGTAAG-3′ for 1st PCR; 5′-TGTGGTTCACTTCTGTAGACAAAGC-3′, 5′-TG TAGTGATACCGGCTAGACC-3′ for 2nd PCR) were used for amplification. The cycling conditions used were as follows: 95 °C for 2 min; 30 cycle (95 °C for 20 s, 61 °C for 20 s, 72 °C for 35 s to 2.5 min); 72 °C for 3 min; hold at 4 °C. PCR products were purified using the GeneJET PCR purification kit (Thermo Fisher), and then digested purified PCR DNA with SphI to assess KI. Different cleavage patterns were detected under 2% agarose gel electrophoresis. After selection with SphI, potential candidates were sequenced and the insertion of specific mutation on Gtf2i gene confirmed. To check Indel (insertion/deletion) rate, $1–2 \times 10^6$ cells were transfected with peSpCas9-mGTF2I using Nucleofector and applied puromycin next day. After 48 h, cells were washed with PBS and fresh medium was added. About 2 weeks later, genomic DNA was isolated from expanded cells and CRISPR/Cas9 target region was amplified with GTF2I-KI-F and -R primers. Five microliters of the amplified DNA was eletrophoresed on 1% agarose gel to confirm single band was produced. Subsequently, PCR products were purified and eluted with 30 μl of the elution buffer and DNA was mixed with 5 μl of 10× NEB buffer 2 and water to a final volume of 50 μl. PCR products were rehybridized with following conditions: 95 °C for 10 min; ramp down to 85 °C at −2 °C/s; 85 °C for 1 min; ramp down to 75 °C at −0.3 °C/s; 75 °C for 1 min; ramp down to 65 °C at −0.3 °C/s; 65 °C for 1 min; ramp down to 55 °C at −0.3 °C/s; 55 °C for 1 min; ramp down to 45 °C at −0.3 °C/s; 45 °C for 1 min; ramp down to 35 °C at −0.3 °C/s; 35 °C for 1 min; ramp down to 25 °C at −0.3 °C/s; 25 °C for 1 min; hold at 4 C. Reannealed DNA was mixed with 1 μl (10 U) T7 endonuclease I (NEB) and incubated at 37 °C for 45 min. Digested products were visualized on a 2% agarose gel and Indel occurrence was estimated with the following formula: Indel (%) = $100 \times [1-(1-\text{fraction}_{cut})^{1/2}]$ [13].

In vivo mouse experiment

Control or KI cells (8×10^6 cells in 20% matrigel) were injected subcutaneously into the right flanks of six-week old athymic nude female mice (Charles River Laboratories; Wilmington, MA, USA). Tumors were measured with caliper to estimate volume ($0.5 \times \text{width}^2 \times \text{length}$) twice a week and all animal experiments were conducted under a protocol approved by the Georgetown University Animal Care Committee.

Metabolic analysis

Cells were grown in normal culture condition or low-glucose condition (5 mM glucose was added in no glucose RPMI-1640 medium) in 15 cm culture dishes. Cells were harvested with cell scraper, and samples were prepared in quintuplicate. For metabolite extraction, the cells were resuspended in 150 µl of chilled 35% water, 25% MeOH, and 40% isopropanol containing internal standards (50 µl of 1 mg/ml 4-nitrobenzoic acid and 10 µl of 1 mg/ml debrisoquine added to 10 ml of 35% water, 25% MeOH, and 40% isopropanol). The cells were given heat shock treatment by plunging the tubes into dry ice for 30 s and immediately into 37 °C water bath for 90 s, followed by sonication for 30 s. The freeze thaw cycle was repeated. The samples were vortexed and incubated on ice for 20 min followed by addition of 150 µl of acetonitrile. The samples were then transferred to −20 °C for overnight incubation and subsequently centrifuged at 4 °C for 20 min at 13,000 rpm. The supernatant was transferred to a MS vial for UPLC TOF MS analysis and the pellets processed for protein quantification. Each sample (2 µl) was injected onto three different columns: a reverse-phase 2.1 × 50 mm Acquity 1.7 µm BEH C18 column (isolate most metabolites) (Waters Corp; Milford, MA, USA), a 2.1 × 100 mm Acquity 1.7 µm CSH C18 column (Waters Corp) and a 2.1 × 100 mm Acquity 1.8 µm HSS T3 column (specific with polar metabolites) (Waters Corp) using an Acquity UPLC system (Waters Corp). The gradient mobile phase for BEH C18 column consisted of solvent A (100% water with 0.1% formic acid), solvent B (100% acetonitrile with 0.1% formic acid), and solvent D (90% isopropanol and 10% acetonitrile with 0.1% formic acid). The column temperature was set at 40 °C and flow rate of 0.4 ml/min. The total run time was 13 min. The gradient started with 95% of solvent A and 5% of solvent B at a ramp of curve 6. At 8 min, it shifted to 98% solvent B and 2% solvent D and stayed until 11 min. From 12 min, the gradient moved to its initial conditions of 95% of solvent A and 5% of solvent B at a ramp of curve 6. The gradient mobile phase for CSH C18 column consisted of solvent A (50% water and 50% acetonitrile with 0.1% formic acid), solvent B (90% isopropanol with 10% acetonitrile and 0.1% formic acid). The column temperature was set to 65 °C and flow rate of 0.45 ml/min. The total run time was 11 min. The gradient started with 60% of solvent A and 40% of solvent B. At 8 min, it shifted to 100% solvent B until 9 min and then back to its initial conditions. The gradient mobile phase for HSS T3 column consisted of solvent A (100% water with 0.1% formic acid) and solvent B (100% methanol with 0.1% formic acid). The column temperature was set at 45 °C and flow rate of 0.4 ml/min. The total run time was 13 min. The gradient started with 98% of solvent A and 2% of solvent B at a ramp of curve 6. At 7.5 min, it shifted to 10% solvent A and 90% solvent B and stayed until 9 min. From 11 min, the gradient moved to its initial conditions of 98% of solvent A and 2% of solvent B. The elution from the column was introduced to quadrupole time-of-flight mass spectrometer (G2-QTof, Waters Corp) by electrospray ionization at a capillary voltage of 3.0 kV for positive mode and 1.5 kV for negative mode. The sampling cone voltage was set at 30 V and the extraction cone at 3.0. The source temperature was set at 120 °C and desolvation temperature at 500 °C. The cone gas flow was maintained at 25 l/h and desolvation gas flow at 1000 l/h. Leucine-encephalin solution in 50% acetonitrile at a concentration of 2 ng/µl was used as a reference mass ($[M + H]+ = 556.2771$ and $[M − H]− = 554.2615$). The data were acquired in centroid mode from mass range of 50–1200 with the software Mass lynx (Waters Corp). Pooled quality controls samples were injected after every ten injections. In addition, protein quantification was performed using Bradford protein analysis. Centroided and integrated mass spectrometry data from the UPLC-TofMS were processed using XCMS (Scripps Institute) to generate a data matrix containing ion intensities, mass to charge (m/z) and retention time values. Data were normalized to internal standard and protein content. Multivariate data analysis was performed using MetaboAnalyst (v4.0). The intracellular lactate levels were measured using the Lactate Colorimetric Assay Kit II (K627–100, BioVision; Milpitas, CA, USA). Cells (2×10^6) were homogenized with 200 µl of assay buffer by pipetting and pelleted by centrifugation (2000 rpm for 3 min) at 4 °C. Then, 10 µl of samples were transferred into 96-well plates and mixed with 40 µl of assay buffer. Samples were incubated for 30 min at room temperature after 50 µl of reaction mix was added, and absorbance (450 nm) was measured. The average zero standard was subtracted as a background from all readings.
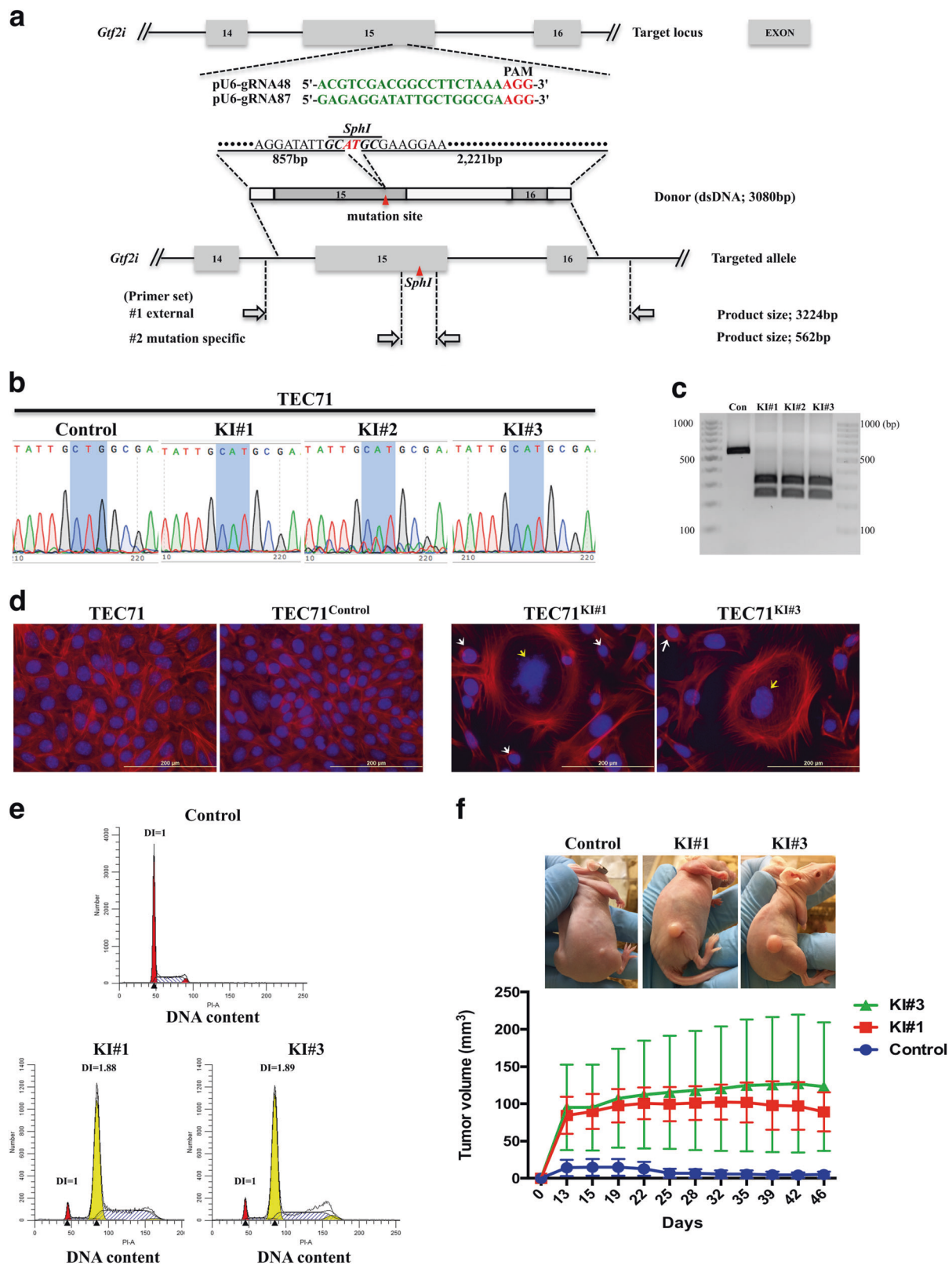
Statistics

Analyses were performed with GraphPad Prism software version 6.0c for Mac (GraphPad; San Diego, CA, USA), and details for analysis are included in figure legends. Data are expressed as the mean ± s.d. and statistical significance was determined by Student's t test or ANOVA test. P value < 0.05 were considered as significant.

Results

Knockin of *Gtf2i* mutation results in cell transformation and tumor formation

The limited availability of primary human TEC lines together with the presence of pseudogenes of *GTF2I* in the

a

Gtf2i — Target locus — EXON

pU6-gRNA48 5'-ACGTCGACGGCCTTCTAAAAGG-3'
pU6-gRNA87 5'-GAGAGGATATTGCTGGCGAAGG-3'
PAM

SphI
AGGATATT*GCATGC*GAAGGAA
857bp   2,221bp
mutation site
Donor (dsDNA; 3080bp)

Gtf2i — Targeted allele

(Primer set)
#1 external   Product size; 3224bp
#2 mutation specific   Product size; 562bp

b

TEC71

Control   KI#1   KI#2   KI#3
TATTGCTGGCGA TATTGCATGCGA TATTGCATGCGA TATTGCATGCGA

c

Con KI#1 KI#2 KI#3

d

TEC71   TEC71^Control   TEC71^KI#1   TEC71^KI#3

e

Control
DI=1
DNA content

KI#1
DI=1.88
DI=1
DNA content

KI#3
DI=1.89
DI=1
DNA content

f

Control   KI#1   KI#3

KI#3
KI#1
Control

human genome, have limited an in depth understanding of the mechanisms of action of *GTF2I*. Given that mouse cells express only the β and δ isoforms of *Gtf2i* [14], and that there are no pseudogenes, we used the CRISPR/Cas9n system for targeted mutational KI as well as to minimize off-target effects [15], in order to examine the function of

◀ **Fig. 1 Cell transformation and in vivo tumorigenic effect of *Gtf2i* mutation. a** Strategy to knockin *Gtf2i* mutation in TEC71 using CRISPR/Cas9n. The *Gtf2i*-specific guide RNA (pU6-gRNA) sequences are in green, and the protospacer-adjacent motif (PAM) sequence is shown in red. The targeted allele is replaced with double-strand DNA template donor containing *SphI* restriction enzyme site (bold italic) and two point mutations (red). A red arrowhead indicates the mutation site of *Gtf2i*. PCR with outward primers (#1) and inward primers (#2) sequentially amplified the genomic region of *Gtf2i* to verify KI. **b** Point mutations (CTG to CAT) of *Gtf2i* identified by Sanger sequencing. TEC71 cells transfected with Cas9n and one gRNA were used as control. **c** DNA fragmentation by *SphI* enzyme was used to verify the correct replacement of *Gtf2i* gene with mutation. One microgram of PCR amplified DNA with primer set #2 was incubated with *SphI* for 3 h and DNA fragments (317 and 245 bp) were analyzed using 2% agarose gel electrophoresis. **d** Cytoskeleton and cell nuclei were stained with Texas Red-X phalloidin and DAPI, respectively, to enable observation of morphological changes. Arrows indicate cellular shape changes associated with cancer: irregular nuclear contour with polylobulation (yellow) or scant cytoplasm (white). Scale bars, 200 μm. **e** DNA-ploidy flow cytometric analysis of KI cells. **f** In vivo xenograft experiment of KI cells and control cells. Tumor volume ($P < 0.0001$) is presented as the means ± s.d. ($n = 10$ mice in each group). Statistical significance was determined by two-way ANOVA.

the *GTF2I* mutation (L424H). We established three KI clones of *Gtf2i* mutation, using a novel strategy (see "Methods"; Fig. 1a and S1A) in TEC71 mTECs. Sanger sequencing and enzyme digestion were performed to confirm precise substitution (CTG > CAT) and insertion of *SphI* site in the targeted alleles, respectively (Fig. 1b, c). The KI cells displayed an irregular size compared with control cells: the average diameter of control cells was 10.2 μm and 99% of the cells were measured at 5.5–15.0 μm. The average diameter of KI cells was 14.8 μm and most of the cells were larger in diameter than control cells (88.6% 10.1–20.0 μm and 7.6% 20.1–30.0 μm, $P < 0.001$ unpaired *t* test) (Fig. S1B). KI cells displayed altered morphology (spindle-shaped elongation, and enlarged cell size) and nuclear shape with chromosomal aneuploidy (Fig. 1d, e and S1C), features which are characteristic of cellular transformation. We then evaluated the tumorigenic potential of *Gtf2i* mutation in vivo. Unlike control cells, KI cells resulted in tumor formation in nude mice while no significant differences were detected in body weight (Fig. 1f and Table S2). Taken together, our results indicate that the *Gtf2i* mutation has oncogenic activity and is tumorigenic.

Gene expression profiling of KI cells

The gene expression profiles of KI cells were examined using expression microarray analysis; KEGG pathway analysis revealed that metabolic and cancer-related pathways were most enriched in KI cells (Fig. 2a–c and Table S3). These included several signaling pathways which are frequently overexpressed in cancer (i.e., VEGF,

Wnt, Hedgehog, and Notch); oncogenes, EMT-related, and antiapoptotic genes. Moreover, expression of genes known to be overexpressed in thymoma such as Fas, Vcam1, and Bcl2 [16, 17] were also observed (Table S4). Furthermore, the expression of genes encoding cell adhesion molecules, tumor suppressors, and cell death inducers was decreased in KI cells (Table S5). We confirmed an increase in VEGF/Wnt/Notch signaling, EMT regulators, oncogenes, anti-apoptotic genes, and a decrease (cell adhesion related genes) in KI cells, using qRT-PCR, (Fig. 2d and S1D). At protein level *Gtf2i* mutation increased expression of VEGF signaling molecules, EMT-related molecules, and proto-oncogenes (Fig. 2e and S1E). Together, these results indicate that mtTFII-I-mediated transcriptomic alterations may contribute to tumorigenesis.

mtTFII-I activates oncogenic pathways in cortical mTECs

To determine whether *Gtf2i* mutation has same effect on cortical TECs, we established a doxycycline (Dox)-inducible system for mtTFII-I expression in TEC100.4 and TEC41.2 cells; because of high expression levels of TFII-I in all the five cell lines that we had available we did not overexpress wtTFII-I (Fig. 3a–c). Then we compared the gene expression profiles of TEC100.4 cells expressing either wtTFII-I (Dox untreated) or mtTFII-I (Dox treated); 3663 genes were identified by expression microarray analysis. Commonly regulated genes were mainly enriched in cancer pathways while mtTFII-I expression had little effect on metabolic pathway (Table S6), therefore we further narrowed down the list of potential targets to specific pathways involved in cancer by mtTFII-I. Expression of 48 genes was coregulated by TFII-I-βmt and TFII-I-δmt (Fig. 3d–f and Table S7–8). Of the 48 genes that are regulated in common, several proto-oncogenes were upregulated by mtTFII-I, similar to the KI cells (Fig. 2).

Protein levels of six proto-oncogenes were further examined by WB. Dox-induced TFII-I-δmt increased c-fos protein levels, however different VEGFR2 expression patterns were detected in mTECs: VEGFR2 protein levels were increased by both isoforms of mtTFII-I in TEC41.2 but only by TFII-I-δmt in TEC100.4. Although the mRNA level was positively regulated by mtTFII-I, WNT2B, and FGFBP1 protein levels were not significantly changed in two mTECs. In addition, c-myc expression was enhanced by mtTFII-I in TEC100.4 (2.1- and 1.4-fold by βmt and δmt, respectively) and in TEC41.2 (2.4- and 1.5-fold by βmt and δmt, respectively) (Fig. 3g). Consistent with the microarray and qRT-PCR results, c-kit protein levels were also elevated by mtTFII-I expression (Fig. 3h). It has been reported that β and δ isoforms of *GTF2I* have distinct roles and subcellular localization, and extracellular stimuli such as serum
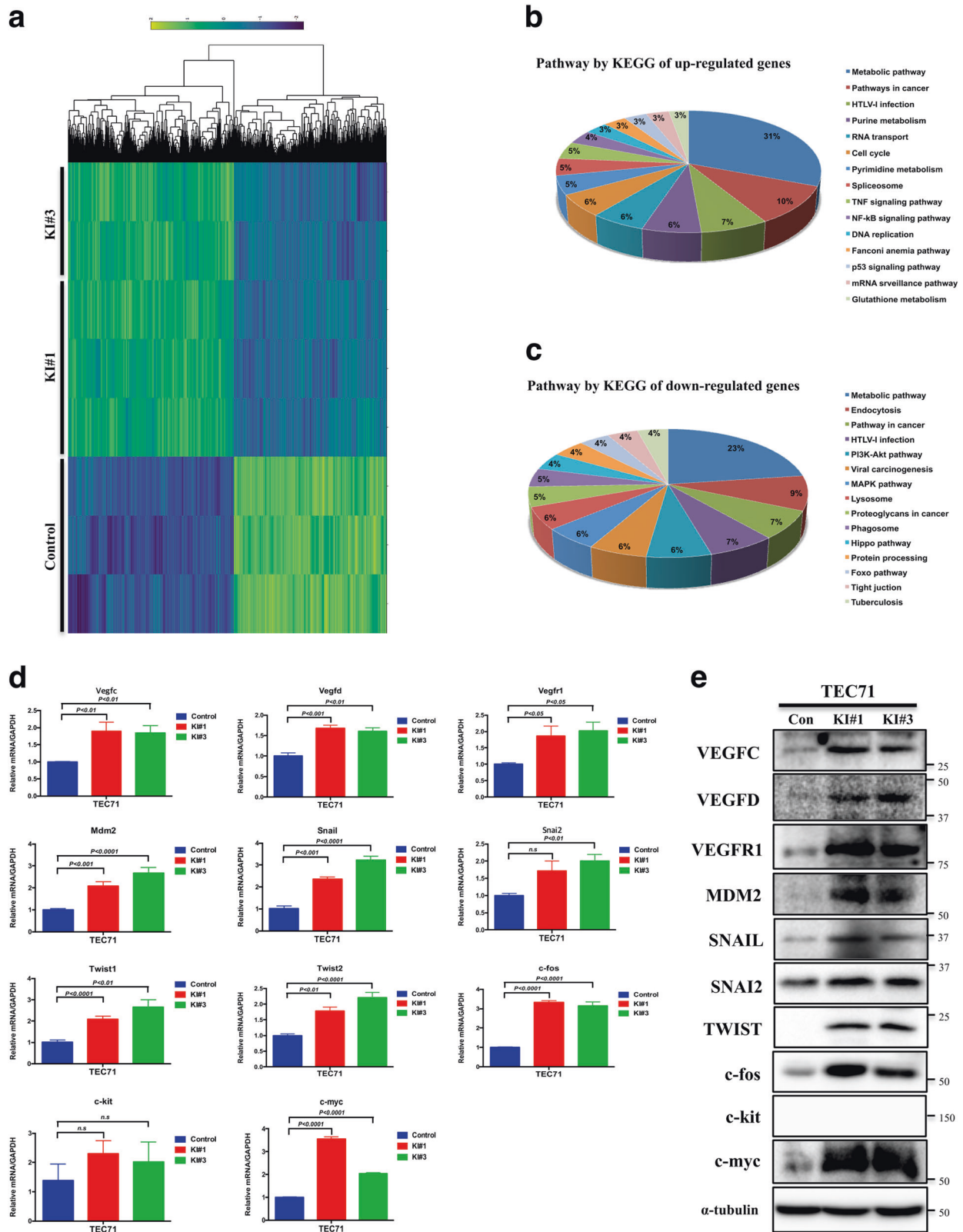
reverses localization of both isoforms [11]. However, similar to a previous report [14], we found no difference in the localization of ectopically expressed TFII-I proteins in both mTECs (cortical and medullary) and NIH-3T3 cells (Fig. S2A–C). These data demonstrate that mutant *Gtf2i* gene expression has the same effect on cortical TECs and

Fig. 2 Oncogenic and EMT-related genes are increased by *Gtf2i* **mutation. a** Heatmap of differentially expressed 6528 genes from two KI cells compared with control cells. The data represent fold change of expression: increased expression (yellow), decreased expression (blue), no change (dark green). **b**, **c** The expression of 6528 transcripts overlapped in the profile. Pathway analysis by KEGG for upregulated (**b**) or downregulated (**c**) genes in common between KI#1 and KI#3 cells. **d** The mRNA expression levels of indicated genes determined by qRT-PCR and normalized by GAPDH expression. All data are means ± s.d. from three independent experiments ($n = 3$), and statistical significance was determined by two-way ANOVA with Sidak's multiple comparisons test. n.s not significant. **e** Comparison for protein levels of ten selected genes between control and KI cells by WB analysis.

induction of oncogene expression by mtTFII-I that may be at the base of the potential tumorigenic activity of *GTF2I* mutation.

Gtf2i mutation confers survival advantage under glucose deprivation

Given that metabolic pathway was strongly altered by *Gtf2i* mutation (Fig. 2) and the primary energy source for normal and tumor cells is glucose, we investigated whether *Gtf2i* mutation influences cell survival in different glucose concentrations. Although *Gtf2i* mutation decreased cell proliferation in normal (11 mM) culture condition, KI cells continued to grow and demonstrated enhanced survival under no and low (1 and 5 mM) glucose conditions (Fig. 4a, b). Reduced glucose consumption based on low cell proliferation of KI cells may contribute to the sensitivity of glucose deprivation at early time points. No or low glucose-induced apoptosis in control cells, as shown by cleavage of PARP and caspase-3, γH2AX expression, and increased sub-G1 fraction (29–59%) while the expression levels of apoptotic markers and the sub-G1 cell populations were relatively low (5.7–28%) in KI cells (Fig. 4c, d and S3A, B). The resistance to low glucose-induced apoptosis in KI cells was further confirmed by TUNEL and FACS analysis (Fig. 4e, f and S3C, D). These results indicate that *Gtf2i* mutation promotes mTECs survival under metabolic stress condition.

Metabolic reprogramming in KI cells by activation of glycolysis and altered lipid biosynthesis

Cancer cells exhibited different metabolic patterns compared with normal cells, at least in part manifested as enhanced glucose metabolism, aerobic glycolysis, lactate production, and high lipid metabolic activities [18]. In order to obtain better insight into *Gtf2i* mutation-induced metabolic shift under normal and glucose-limited condition, we performed metabolic profiling using LC/MS. In total, 17,512 and 21,005 metabolites were altered in two KI cells compared with control cells. The major difference between KI cells cultured

in normal vs low glucose was in lipids (CSH column, right middle) (Fig. 5a) while only a few glycolysis and TCA cycle-related metabolites were detected by LC/MS (Table S9A). Metabolite set enrichment analysis demonstrated that the *Gtf2i* mutation induced marked intracellular metabolic changes (Fig. S4). In particular, the pathway of arachidonic acid (AA) and sphingolipid metabolism was significantly altered in KI cells as compared with controls regardless of cell culture condition (Fig. S5 and Table S9B-E). Western blot (WB) analysis in KI cells cultured under normal medium showed increased expression of four glycolytic enzymes: Hexokinase I, PFKFB2 (6-phosphofructo-2-kinase/fructose-2,6-biphosphatase 2), PFKP (phosphofructokinase, platelet), and Enolase-2. Intriguingly, these enzymes were also induced in glucose-limited conditions with the exception of Hexokinase I (Fig. 5b). The levels of lactate, the end product of glycolysis, were increased regardless of glucose concentration in KI cells (Fig. 5c). Glucose also supports fatty acid (FA) production through the synthesis of citrate and its conversion to acetyl-coenzyme A, the major precursor of lipid biosynthesis. Not only AA, which is polyunsaturated FA, but also many different types of lipids, including eicosanoids and sphingolipids, can be generated from FA [19]. AA is converted into prostaglandins by cyclooxygenases (COX), and we found that COX-2 levels were upregulated in KI cells irrespective of the culture conditions (Fig. 5b). Viewed collectively, these results suggest that *Gtf2i* mutation activates glycolysis and enhances lipid content in mTECs (Fig. 5d).

COX-2 is essential for Gtf2i mutation-induced cell survival and transformation

We generated stable KD cell lines to investigate the role of PFKFB2 and COX-2 in survival under metabolic stress. No or low glucose-induced apoptosis in two COX-2 KD cells, as shown by cleavage of PARP and caspase-3, γH2AX expression, marked increase of sub-G1 fraction and number of apoptotic cells (Fig. 6a–c and S6A–D), whereas cleavage of PARP and caspase-3 was not induced by PFKP or ENO2 KD in KI cells (Fig. S6E). Expression of apoptosis-related genes was only slightly induced by low glucose in PFKFB2 KD cells, and these cells did not exhibit evidence of apoptosis by flow cytometry analysis (Fig. 6a–c). Neither COX-2 nor PFKFB2 are required for survival under metabolic stress-induced apoptosis in control cells (Fig. S6F). Next, we investigated whether COX-2 or PFKFB2 is required for cellular transformation of KI cells induced by *Gtf2i* mutation in mTECs. COX-2 KD resulted in diminished actin formation and cells displayed typical epithelial morphology (Fig. 6d). Moreover, VIMENTIN and TWIST expression of KI cells was significantly decreased in COX-2 KD cells (Fig. 6e, f). In contrast, PFKFB2 KD had no effect
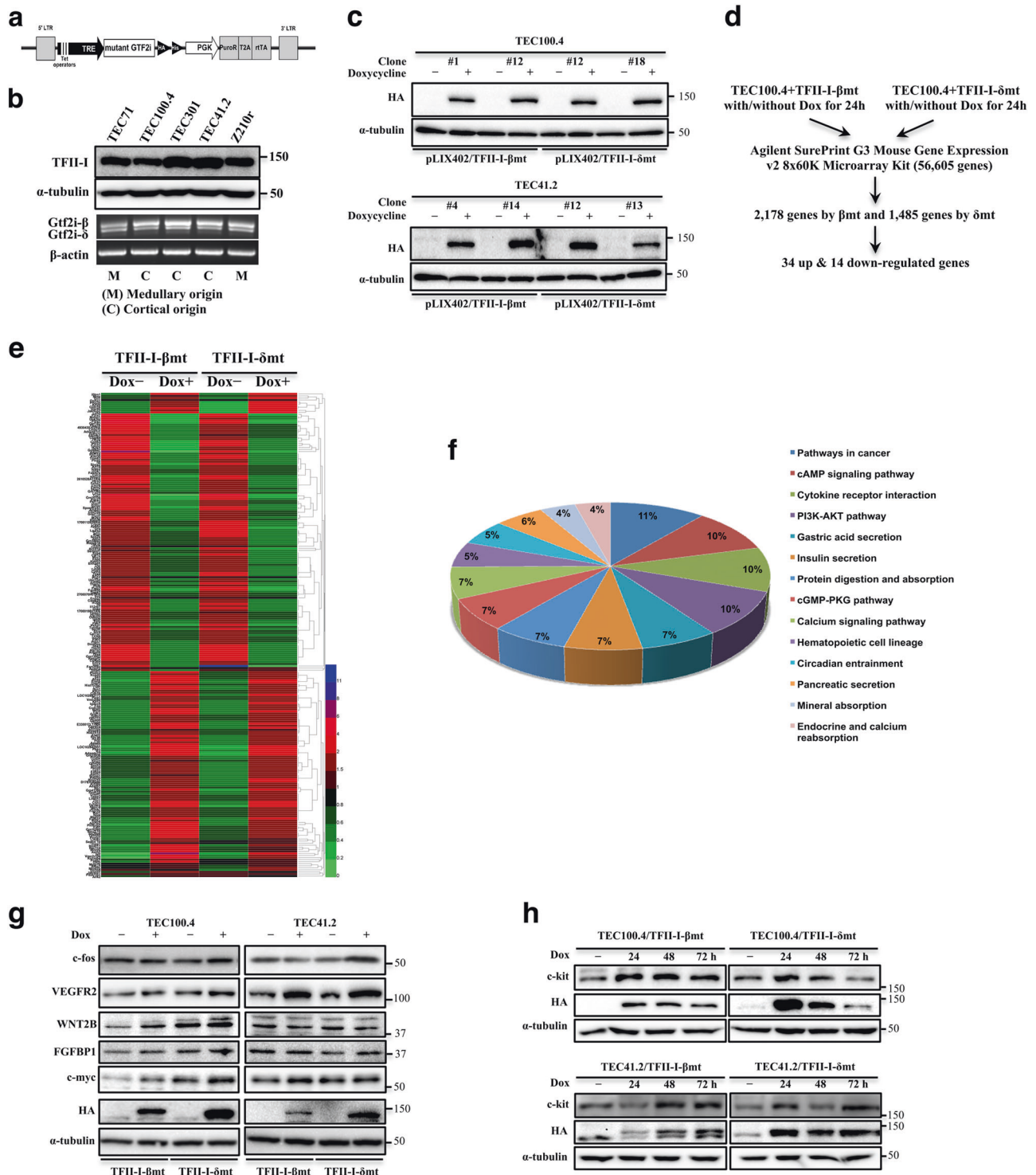
Fig. 3 Mutant TFII-I induces oncogene expression. a Diagram of the inducible expression system of pLIX402. **b** TFII-I protein level (upper panel) and mRNA level of *Gtf2i*-β and -δ isoforms (lower panel) in mTECs. **c** Cells were incubated with/without doxycycline (Dox) for 24 h, and the inducible expression system was assessed by HA antibody. **d** Schematic representation of microarray anaylsis. **e** Heatmap of 235 differentially expressed genes between mtTFII-I-inducible TEC100.4 cells treated with/without Dox. The data represent fold change of expression: increased expression (red and blue), decreased expression (green), no change (black). **f** Pathway analysis for 235 coregulated genes by TFII-I-β and -δmt. **g** Cells were incubated with/without Dox for 24 h and protein levels were evaluated by WB analysis. ImageJ software was used to quantify signal intensity. **h** Dox-treated cells were harvested at indicated incubation time points and evaluated for c-kit levels by WB.
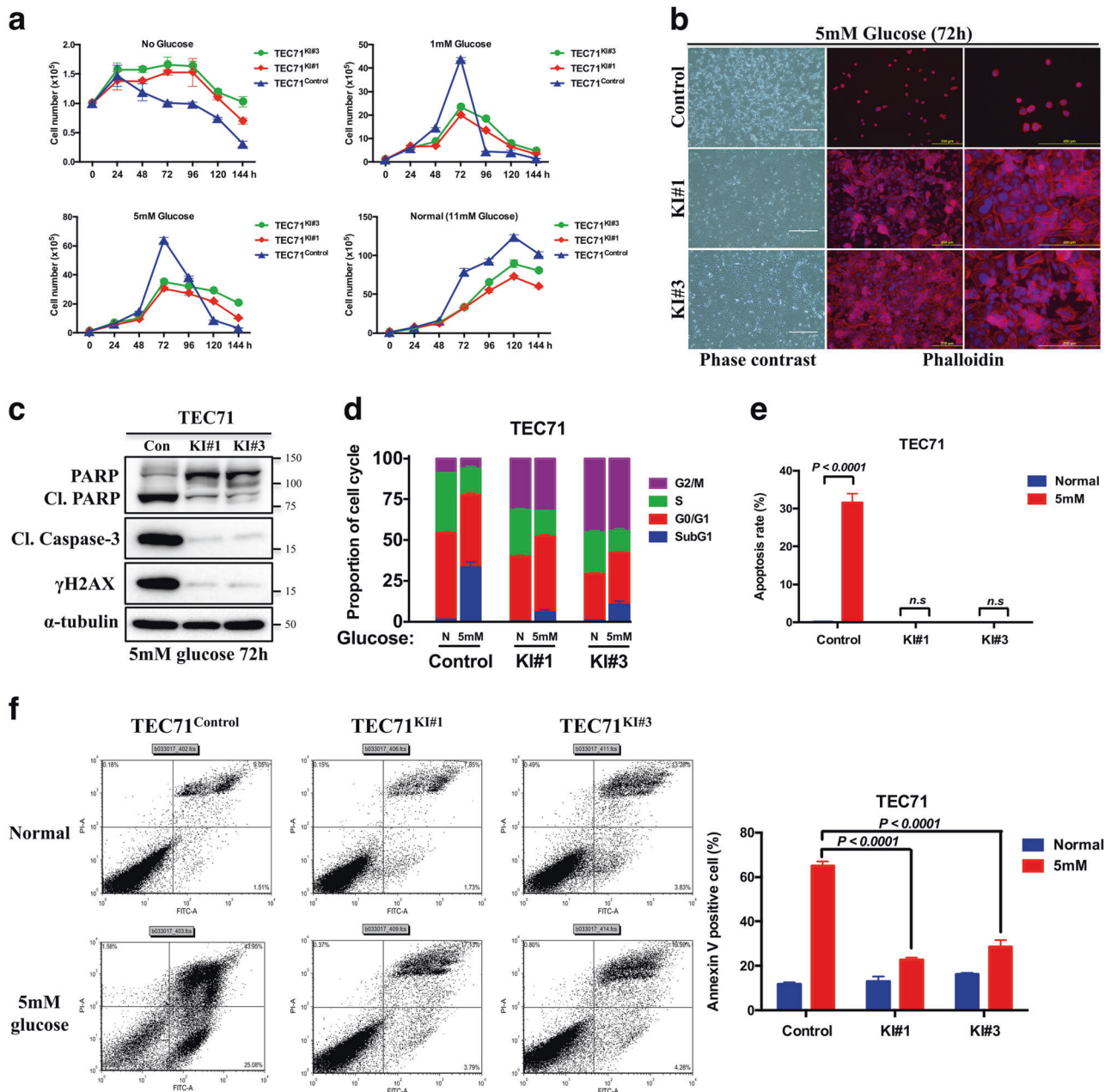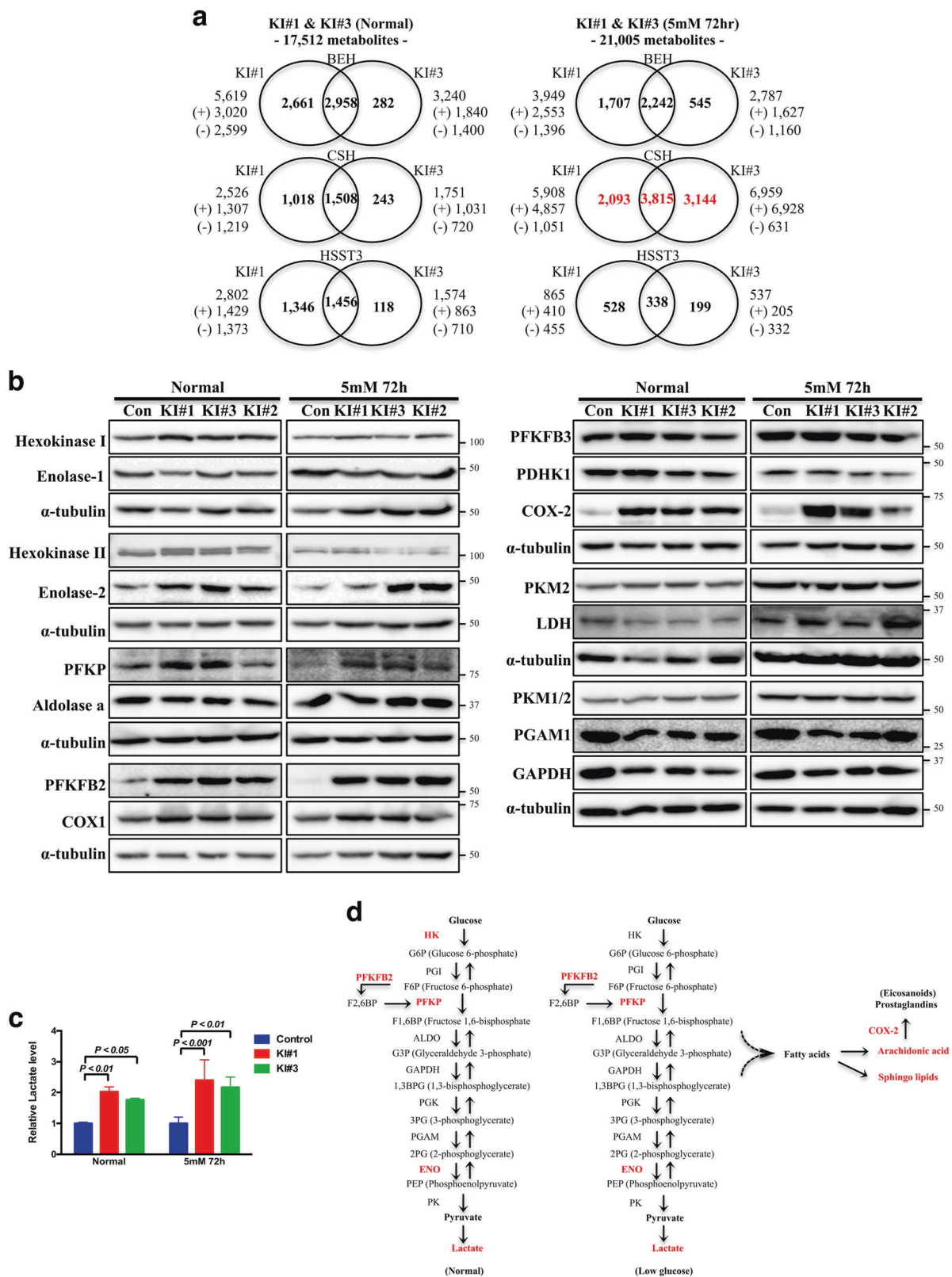
Fig. 4 *Gtf2i* mutation confers survival advantage under glucose deprivation. **a** Effect of *Gtf2i* mutation on the proliferation of TEC71 cells under different glucose conditions. Cell numbers were determined with trypan blue at indicated time points. Error bars represent s.d. of three replicate samples. **b** Representative images of control and KI cells under low glucose examined with phase contrast microscopy using an EVOS imaging system (AMG) (left); immunofluorescence using Texas Red-X phalloidin (red) and counterstained with DAPI (blue) (right). Scale bar, 200–400 μm. **c** WB analysis of PARP, cleaved caspase-3, and γH2AX in KI cells. **d** Cells were grown in normal (N) or low glucose (5 mM) medium for 72 h and cell cycle distribution was determined by flow cytometry. **e** Representative histogram showing the percentage of apoptotic cells (TUNEL-positive cells; Fig. S3C). **f** Apoptotic rate was assessed by flow cytometry with Annexin V/PI staining in cells grown in normal or low glucose condition for 72 h. Data are means ± s.d. from three independent experiments (*n* = 3), and statistical significance was determined by two-way ANOVA. n.s not significant.

on morphology and VIMENTIN expression in KI cells while cells showed epithelial-like cell formation and a reduction of TWIST (Fig. 6d–f). These results suggest that *Gtf2i* mutation promotes cell survival and induces cellular transformation through COX-2 expression in mTECs.

Enhanced tolerance to DNA damage associated with *Gtf2i* mutation

Since TFII-I is required for DNA translesion synthesis and increases DNA damage tolerance [20], we compared DNA

a

KI#1 & KI#3 (Normal)
- 17,512 metabolites -

BEH

KI#1 **2,661** | **2,958** | **282** KI#3
5,619 | | | 3,240
(+) 3,020 | | | (+) 1,840
(-) 2,599 | | | (-) 1,400

CSH

KI#1 **1,018** | **1,508** | **243** KI#3
2,526 | | | 1,751
(+) 1,307 | | | (+) 1,031
(-) 1,219 | | | (-) 720

HSST3

KI#1 **1,346** | **1,456** | **118** KI#3
2,802 | | | 1,574
(+) 1,429 | | | (+) 863
(-) 1,373 | | | (-) 710

KI#1 & KI#3 (5mM 72hr)
- 21,005 metabolites -

BEH

KI#1 **1,707** | **2,242** | **545** KI#3
3,949 | | | 2,787
(+) 2,553 | | | (+) 1,627
(-) 1,396 | | | (-) 1,160

CSH

KI#1 **2,093** | **3,815** | **3,144** KI#3
5,908 | | | 6,959
(+) 4,857 | | | (+) 6,928
(-) 1,051 | | | (-) 631

HSST3

KI#1 **528** | **338** | **199** KI#3
865 | | | 537
(+) 410 | | | (+) 205
(-) 455 | | | (-) 332

b

c

d

damage response to test whether mtTFII-I protects cells from DNA damage-induced apoptosis. KI cells were more resistant to UV-mediated (4–12 J/m^2) cell death and showed better survival than control cells (Fig. 7a, b and S7). To obtain further evidence for the role of *Gtf2i* mutation in DNA damage response, cells were exposed to cisplatin or

doxorubicin treatment and KI cells were more resistant compared with control cells (Fig. 7c). Different DNA-damaging sources induced the expression of apoptotic markers (cleaved PARP/Caspase-3 and γH2AX) in control cells but less in KI cells, with the exception of γH2AX expression induced by doxorubicin, which is known to inhibit the progression of topoisomerase II (Fig. 7d). DNA damage activates the tumor suppressor p53 and causes cell cycle arrest to trigger apoptosis. We observed that both total p53 and phospho-p53 (Ser15) levels in KI cells were increased more than in control cells by UV, cisplatin, and doxorubicin (Fig. 7e). KI cells also expressed high levels of p21, a cell cycle inhibitor, than control cells exposed to DNA damage whereas such differences were not observed for p16. Because transcription of the antiapoptotic regulator Bcl2 was increased in KI cells (Fig. S1D and Table S4), we therefore examined whether antiapoptotic genes can be induced by DNA damage in KI cells. KI cells expressed higher levels of Bcl2 and Bcl-xL in response to UV, cisplatin, and doxorubicin treatment, compared with control cells (Fig. 7e). Together, these results suggest that *Gtf2i* mutation confers a survival advantage to DNA damage-induced cell death in mTECs.

Discussion

Here we have demonstrated that mtTFII-I induces the expression of oncogenes, of several glycolytic enzymes, lactate production, and AA metabolism are positively regulated by *Gtf2i* mutation. *Gtf2i* mutation caused cellular transformation, aneuploidy, and tumorigenicity in vivo, and conferred a survival advantage against nutrient deprivation and DNA damage. We also present evidence that COX-2 expression is required for cellular transformation and survival of mTECs induced by *Gtf2i* mutation. Based on these findings, we propose that *GTF2I* L424H mutation is an oncogenic driver mutation responsible for the initiation of tumorigenesis in TECs (Fig. S8).

Several transcription factors have been identified to be oncogenic through fusion with other proteins, or deregulated expression due to mutations [21]. However, there are very few tumors that are characterized by one dominant

genetic abnormality [22]. *GTF2I* has been studied mainly in relation to a genetic syndrome (Williams–Beuren), autoimmune diseases, and embryonic development [9], while only a few studies have identified an association with cancer with substantial experimental evidence, to date. In previous studies we have shown that higher c-fos expression is detected in human TETs that harbor *GTF2I* mutation than *GTF2I* wild type, and the *GTF2I* Leu > His may augment its activity or gain novel functions by recruiting new interaction partners [7]. In addition, *myc* was found to be highly expressed in mouse thymic tumors [23]. In the present study, we found that both mRNA and protein levels of *c-fos* and *c-myc* are upregulated by mtTFII-I. Structural chromosomal abnormalities and aneuploidy are well-defined characteristics of cancer and can predispose to tumor development [24]. EMT is an essential morphologic transformation for cancer development and progression. Hognas et al. showed that aneuploidy facilitates oncogenic transformation via Twist2 [25], and high prevalence of aneuploidy was detected in thymoma [8]. In addition, type A and AB thymomas are strongly positive for vimentin [26] and Slug is overexpressed in 51% (51/100) of thymoma tissues [27]. Similar to these reports, we observed higher levels of *Twist*, *Snail*, and *Vimentin* expression in *GTF2I* mutant thymomas than *GTF2I* wild-type thymomas by RNA-seq; our observation in transcriptional changes is consistent with transcriptional differences in human thymic tumors according to the presence/absence of *GTF2I* mutation (Fig. S9–10). Here, we showed that *Gtf2i* mutation causes severe aneuploidy and EMT in mTECs. Furthermore, both *c-fos* and *myc* expressions are thought to contribute to transformation of TECs [28], indicating that *GTF2I* mutation is the earliest driving force for tumor development through chromosomal instability and EMT.

Recent studies revealed that dysregulated metabolism is associated with EMT, and metabolic reprogramming has been observed in relation to mutations in oncogenes or tumor suppressors, and altered energy metabolism is a hallmark of cancer [29, 30]. Prostaglandins are a group of lipids derived from the sequential oxygenation of AA by COX-1 and COX-2: whereas COX-1 is diffusely expressed in most tissues, COX-2 is inducible and increased expression has been detected in various cancer cell types and tissues including all primary epithelial cancers. Although COX-2 is overexpressed in most TETs and in the medullary epithelial cells only [31], the underlying molecular mechanisms by which COX-2 expression is regulated in TETs remain unclear. Numerous functional regulatory elements were identified in the human and mouse COX-2 gene promoters, including cyclic AMP response element, sterol response element, CAAT enhancer binding protein motif, SP1/NF-kB/AP-1 site, E-box, and TATA box [32]. TFII-I interacts with the E-box that is recognized by USF
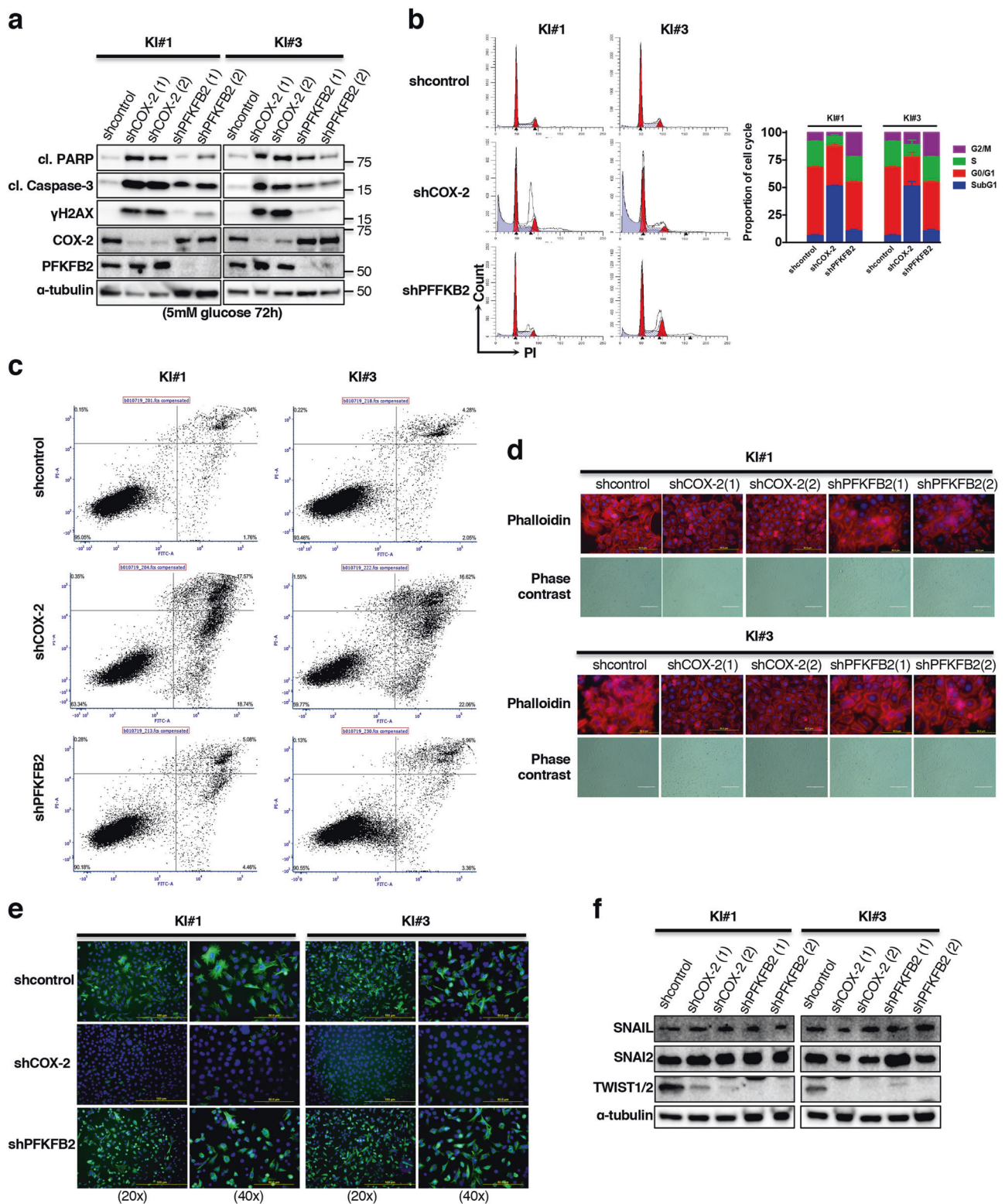
(upstream transcription factor) and TFII-I was identified as part of a co-regulatory protein complex with Sp1/3 and USF1 that represses the SSeCKS gene expression [11, 33]. Because Sp1 site is close to the E-box element at position −52/−47 in the mouse COX-2 promoter in the

TRANSFAC database, it is conceivable that COX-2 gene expression might be regulated by mtTFII-I through similar mechanisms as described for SSeCKS gene expression. COX-2 favors tumorigenesis by promoting angiogenesis, cell proliferation, activation of transcription factors that

◀ **Fig. 6 COX-2 contributes to cell survival and transformation mediated by *Gtf2i* mutation. a** Cells were grown in low glucose (5 mM) medium for 72 h and protein levels were evaluated by WB. **b** Cells were grown in low glucose (5 mM) medium for 72 h and cell cycle distribution was determined by flow cytometry (left), the percentage in each phase of the cell cycle is shown (right). Data are means ± s.d. from three independent experiments ($n = 3$), and statistical significance was determined by two-way ANOVA. **c** Apoptotic rate was assessed by flow cytometry with Annexin V/PI staining in cells grown in low glucose (5 mM) condition for 72 h. **d** Representative images of KD cells stained with Texas Red-X phalloidin (red) and DAPI (blue). Cell images under normal culture dish are observed by phase contrast microscope. Scale bar, 50 μm (palloidin) or 200 μm (phase contrast). **e** Immunostaining for VIMENTIN (green), DAPI was used for nuclear staining (blue). Scale bars, 100 μm (20×) or 50 μm (40×). **f** WB analysis for SNAIL, SNAI2, and TWIST in COX-2 or PFKFB2 KD cell lines.

regulate EMT, and prevention of apoptosis [34, 35]. In line with this, we demonstrated that COX-2 is upregulated by *Gtf2i* mutation and speculated that alterations in the lipidic metabolism play a pivotal role in cell survival and carcinogenesis. Indeed, we discovered that *Gtf2i* mutation confers survival and transformation of mTECs through COX-2 and TWIST expression. Given that EMT is shown to control metabolic reprogramming [36], COX-2/TWIST-induced EMT is a possible mechanism in play in tumorigenesis of mTECs by *Gtf2i* mutation.

TFII-I connected DNA polymerase (Pol ζ) to PCNA (proliferating cell nuclear antigen) and facilitated translesion synthesis; TFII-I depletion enhanced UV or cisplatin sensitivity, and ectopic TFII-I expression reduced DNA double-strand break in human cells [20]. DNA damage in response to oncogenic stress activated p53 and activation of
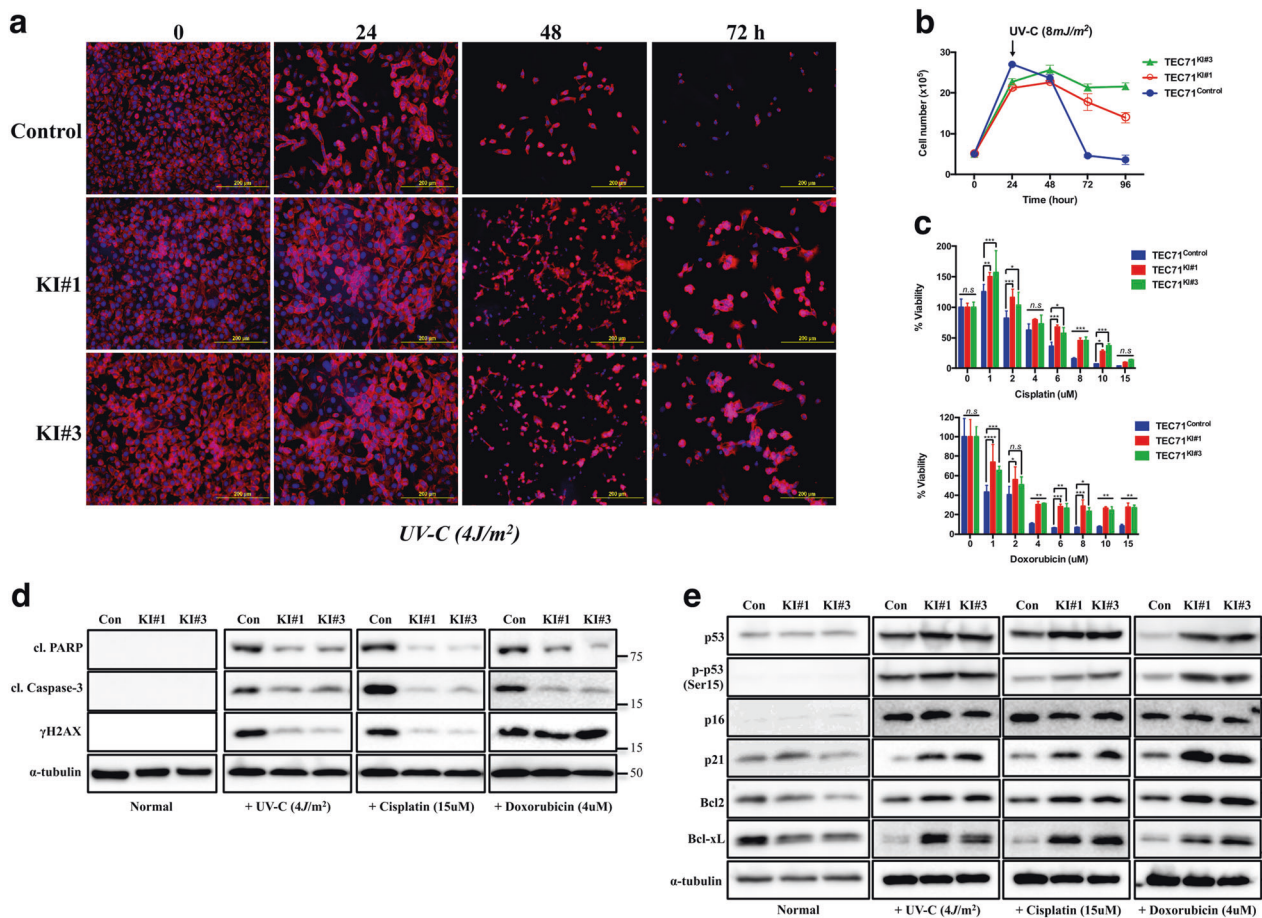
Fig. 7 *Gtf2i* mutation confers DNA damage resistance. a Representative images of control and KI cells under UV exposure stained with Texas Red-X phalloidin (red) and counterstained with DAPI (blue). Scale bar, 200 μm. **b** Cells (5×10^5) were plated in 6 cm dish and cell numbers were determined with trypan blue at indicated time points. Error bars represent s.d. of three replicate samples. **c** Cells were treated at indicated concentrations of cisplatin (upper panel) or doxorubicin (low panel) and cell viability was measured by the CCK-8 assay after 48 h incubation. Data are means ± s.d. from three independent experiments ($n = 4$). Statistically significant differences compared with control are denoted as *$P < 0.05$; **$P < 0.01$; ***$P < 0.001$; ****$P < 0.0001$; n.s not significant by two-way ANOVA with Sidak's multiple comparisons test. **d, e** Protein levels were evaluated by WB analysis. Cells were irradiated with UV or exposed to either cisplatin or doxorubicin, and harvested after 24 h.

p53-mediated transcription is a critical cellular mechanism of tumor suppression [37]. p21 has been shown to be regulated by p53-dependent and -independent mechanisms following stress and p21 expression caused cell cycle arrest. However, normal function of p21 was to protect thymic tumor cells against ionizing radiation and p21 was not essential for p53-dependent apoptosis in mouse thymocytes [38]. In addition, increasing evidence suggests that p21 is a negative regulator of apoptosis, through: (1) nuclear translocation and binding to chromatin-bound PCNA for DNA repair, (2) interaction of p21 with pro-apoptotic molecules in the cytoplasm [39]. Although the intracellular localization of p21 and p53 was not altered by DNA damage in KI cells (Fig. S11), our data led us to presume that mtTFII-I confers DNA damage resistance through antiapoptotic gene expression, DNA repair, or inhibition of p53 transactivity by MDM2 [40] in TECs. In keeping with our findings, pathway analysis demonstrated lower expression of genes involved in apoptosis, cell cycle, and DNA damage response in *GTF2I* mutant tumors compared with *GTF2I* wild-type tumors [8].

In summary, here we propose that *GTF2I* mutation can directly contribute to tumor formation in TECs. Since we have identified the missense mutation of *GTF2I*, other groups confirmed this specific mutation [41, 42] including TCGA project, which suggested to be a founder mutation occurring early in tumor development [8]. Moreover, thymus specific *GTF2I* L424H mutation was recently identified as one of 1165 statistically significant recurrent mutations in 24,592 human tumor samples [43]. Taken together, all our observations underscore the *GTF2I* mutation as a specific molecular marker for TETs. The study of the precise mechanisms by which mtTFII-I regulates target gene expression and the exact functional differences between TFII-I-βmt and TFII-I-δmt will need to be addressed.

Compliance with ethical standards

Conflict of interest The authors declare that they have no conflict of interest.

References

1. Engels EA. Epidemiology of thymoma and associated malignancies. J Thorac Oncol. 2010;5:S260–265.
2. De Jong WK, Blaauwgeers JL, Schaapveld M, Timens W, Klinkenberg TJ, Groen HJ. Thymic epithelial tumours: a population-based study of the incidence, diagnostic procedures and therapy. Eur J Cancer. 2008;44:123–30.
3. Marx A, Chan JK, Coindre JM, Detterbeck F, Girard N, Harris NL, et al. The 2015 World Health Organization classification of tumors of the thymus: continuity and changes. J Thorac Oncol. 2015;10:1383–95.
4. Venuta F, Anile M, Diso D, Vitolo D, Rendina EA, De Giacomo T, et al. Thymoma and thymic carcinoma. Eur J Cardiothorac Surg. 2010;37:13–25.
5. Scorsetti M, Leo F, Trama A, D'Angelillo R, Serpico D, Macerelli M, et al. Thymoma and thymic carcinomas. Crit Rev Oncol Hematol. 2016;99:332–50.
6. Kelly RJ, Petrini I, Rajan A, Wang Y, Giaccone G. Thymic malignancies: from clinical management to targeted therapies. J Clin Oncol. 2011;29:4820–7.
7. Petrini I, Meltzer PS, Kim IK, Lucchi M, Park KS, Fontanini G, et al. A specific missense mutation in GTF2I occurs at high frequency in thymic epithelial tumors. Nat Genet. 2014;46:844–9.
8. Radovich M, Pickering CR, Felau I, Ha G, Zhang H, Jo H, et al. The integrated genomic landscape of thymic epithelial tumors. Cancer Cell. 2018;33:244–58 e210.
9. Roy AL. Pathophysiology of TFII-I: old guard wearing new hats. Trends Mol Med. 2017;23:501–11.
10. Hinsley TA, Cunliffe P, Tipney HJ, Brass A, Tassabehji M. Comparison of TFII-I gene family members deleted in Williams–Beuren syndrome. Protein Sci. 2004;13:2588–99.
11. Roy AL. Biochemistry and biology of the inducible multifunctional transcription factor TFII-I: 10 years later. Gene. 2012;492:32–41.
12. Chu VT, Weber T, Wefers B, Wurst W, Sander S, Rajewsky K, et al. Increasing the efficiency of homology-directed repair for CRISPR-Cas9-induced precise gene editing in mammalian cells. Nat Biotechnol. 2015;33:543–8.
13. Ran FA, Hsu PD, Wright J, Agarwala V, Scott DA, Zhang F. Genome engineering using the CRISPR-Cas9 system. Nat Protoc. 2013;8:2281–308.
14. Hakre S, Tussie-Luna MI, Ashworth T, Novina CD, Settleman J, Sharp PA, et al. Opposing functions of TFII-I spliced isoforms in growth factor-induced gene expression. Mol Cell. 2006;24:301–8.
15. Ran FA, Hsu PD, Lin CY, Gootenberg JS, Konermann S, Trevino AE, et al. Double nicking by RNA-guided CRISPR Cas9 for enhanced genome editing specificity. Cell. 2013;154:1380–9.
16. Park SH, Kim HK, Kim H, Ro JY. Apoptosis in thymic epithelial tumors. Pathol Res Pract. 2002;198:461–7.
17. Alexander M, Hans KM-H. Epithelial tumors of the thymus: pathology, biology, treatment. New York: Plenum Press; 1997.
18. Beloribi-Djefaflia S, Vasseur S, Guillaumond F. Lipid metabolic reprogramming in cancer cells. Oncogenesis. 2016;5:e189.
19. Baenke F, Peck B, Miess H, Schulze A. Hooked on fat: the role of lipid synthesis in cancer metabolism and tumour development. Dis Model Mech. 2013;6:1353–63.
20. Fattah FJ, Hara K, Fattah KR, Yang C, Wu N, Warrington R, et al. The transcription factor TFII-I promotes DNA translesion synthesis and genomic stability. PLoS Genet. 2014;10:e1004419.
21. Lee TI, Young RA. Transcriptional regulation and its misregulation in disease. Cell. 2013;152:1237–51.

22. Tiacci E, Trifonov V, Schiavoni G, Holmes A, Kern W, Martelli MP, et al. BRAF mutations in hairy-cell leukemia. N Engl J Med. 2011;364:2305–15.

23. Conacci-Sorrell M, Ngouenet C, Anderson S, Brabletz T, Eisenman RN. Stress-induced cleavage of Myc promotes cancer cell survival. Genes Dev. 2014;28:689–707.

24. Gordon DJ, Resio B, Pellman D. Causes and consequences of aneuploidy in cancer. Nat Rev Genet. 2012;13:189–203.

25. Hognas G, Hamalisto S, Rilla K, Laine JO, Vilkki V, Murumagi A, et al. Aneuploidy facilitates oncogenic transformation via specific genetic alterations, including Twist2 upregulation. Carcinogenesis. 2013;34:2000–9.

26. Liu B, Rao Q, Zhu Y, Yu B, Zhu HY, Zhou XJ. Metaplastic thymoma of the mediastinum. A clinicopathologic, immunohistochemical, and genetic analysis. Am J Clin Pathol. 2012;137:261–9.

27. Zhang T, Chen XU, Chu X, Shen YI, Jiao W, Wei Y, et al. Slug overexpression is associated with poor prognosis in thymoma patients. Oncol Lett. 2016;11:306–10.

28. Scheijen B, Bronk M, van der Meer T, De Jong D, Bernards R. High incidence of thymic epithelial tumors in E2F2 transgenic mice. J Biol Chem. 2004;279:10476–83.

29. Hanahan D, Weinberg RA. Hallmarks of cancer: the next generation. Cell. 2011;144:646–74.

30. Liu M, Quek LE, Sultani G, Turner N. Epithelial-mesenchymal transition induction is associated with augmented glucose uptake and lactate production in pancreatic ductal adenocarcinoma. Cancer Metab. 2016;4:19.

31. Rieker RJ, Joos S, Mechtersheimer G, Blaeker H, Schnabel PA, Morresi-Hauf A, et al. COX-2 upregulation in thymomas and thymic carcinomas. Int J Cancer. 2006;119:2063–70.

32. Kang YJ, Mbonye UR, DeLong CJ, Wada M, Smith WL. Regulation of intracellular cyclooxygenase levels by gene transcription and protein degradation. Prog Lipid Res. 2007;46:108–25.

33. Bu Y, Gao L, Gelman IH. Role for transcription factor TFII-I in the suppression of SSeCKS/Gravin/Akap12 transcription by Src. Int J Cancer. 2011;128:1836–42.

34. Koki AT, Khan NK, Woerner BM, Seibert K, Harmon JL, Dannenberg AJ, et al. Characterization of cyclooxygenase-2 (COX-2) during tumorigenesis in human epithelial cancers: evidence for potential clinical utility of COX-2 inhibitors in epithelial cancers. Prostaglandins Leukot Ess Fat Acids. 2002;66:13–18.

35. Majumder M, Landman E, Liu L, Hess D, Lala PK. COX-2 elevates oncogenic miR-526b in breast cancer by EP4 activation. Mol Cancer Res. 2015;13:1022–33.

36. Jiang L, Xiao L, Sugiura H, Huang X, Ali A, Kuro-o M, et al. Metabolic reprogramming during TGFbeta1-induced epithelial-to-mesenchymal transition. Oncogene. 2015;34:3908–16.

37. Halazonetis TD, Gorgoulis VG, Bartek J. An oncogene-induced DNA damage model for cancer development. Science. 2008;319:1352–5.

38. Gartel AL, Tyner AL. The role of the cyclin-dependent kinase inhibitor p21 in apoptosis. Mol Cancer Ther. 2002;1:639–49.

39. Cazzalini O, Scovassi AI, Savio M, Stivala LA, Prosperi E. Multiple roles of the cell cycle inhibitor p21(CDKN1A) in the DNA damage response. Mutat Res. 2010;704:12–20.

40. Hernandez-Monge J, Rousset-Roman AB, Medina-Medina I, Olivares-Illana V. Dual function of MDM2 and MDMX toward the tumor suppressors p53 and RB. Genes Cancer. 2016;7:278–87.

41. Feng Y, Lei Y, Wu X, Huang Y, Rao H, Zhang Y, et al. GTF2I mutation frequently occurs in more indolent thymic epithelial tumors and predicts better prognosis. Lung Cancer. 2017;110:48–52.

42. Grajkowska W, Matyja E, Kunicki J, Szymanska S, Marx A, Weis CA, et al. AB thymoma with atypical type A component with delayed multiple lung and brain metastases. J Thorac Dis. 2017;9: E808–E814.

43. Chang MT, Bhattarai TS, Schram AM, Bielski CM, Donoghue MTA, Jonsson P, et al. Accelerating discovery of functional mutant alleles in cancer. Cancer Discov. 2018;8:174–83.